Research Square

Preprints are preliminary reports that have not undergone peer review.
They should not be considered conclusive, used to inform clinical practice,
or referenced by the media as validated information.

Height ratio-dependent creep failure of coal-rock composites: A multi-scale analysis integrating stepwise creep, AE monitoring, and SEM characterization

Fei Ke
China University of Mining and Technology
Yanlong Chen
chenyanlong@cumt.edu.cn

China University of Mining and Technology
Peng Wu
Xuzhou University of Technology
Hai Pu
China University of Mining and Technology
Yuheng Wang
Emergency Management and Assurance Center of Ordos
Pengjiao Zhang
China Shenhua Group Zhungeer Energy Co., Ltd

Research Article

Keywords: rock-to-coal height ratio, combinations, long-term strength, acoustic emission characteristics

Posted Date: June 24th, 2026

DOI: https://doi.org/10.21203/rs.3.rs-9753578/v1

License: This work is licensed under a Creative Commons Attribution 4.0 International License.
Read Full License

Additional Declarations: No competing interests reported.

Height ratio-dependent creep failure of coal-rock composites: A multi-scale analysis integrating stepwise creep, AE monitoring, and SEM characterization

Fei Ke[1], Yan long Chen[1*], Peng Wu[2*], Hai Pu[1], Yu heng Wang[3], Pengjiao Zhang[4]

[1] *State Key Laboratory of Intelligent Construction and Healthy Operation and Maintenance of Deep Underground Engineering, China University of Mining & Technology, Xuzhou 221116, China*

[2] *School of Physics and New Energy, Xuzhou University of Technology, Xuzhou, Jiangsu 221018, China.*

[3] *Emergency Management and Assurance Center of Ordos，Ordos，Inner Mongolia 017004，China.*

[4] *China Shenhua Group Zhungeer Energy Co., Ltd, Ordos, 010300, China*

* Correspondence: chenyanlong@cumt.edu.cn (Y. Chen), pengw@xzit.edu.cn (P. Wu)

Abstract:

The long-term stability of coal pillars in underground stopes and open-pit slopes depends critically on the creep behavior of coal–rock combinations, wherein the rock-to-coal height ratio (K_{rc}) exerts a governing yet insufficiently characterized influence. In this study, stepwise creep tests, scanning electron microscopy observations, and acoustic emission tests were conducted on five types of specimens: pure coal (0:1), three composite specimens with height ratios of 1:3, 1:1, and 3:1, and pure rock (1:0). The influence of the K_{rc} on creep deformation, long-term strength, and Acoustic emission crack evolution was systematically investigated. Three principal findings emerged. First, irrespective of K_{rc}, the creep failure stress consistently approached 90% of the peak uniaxial compressive strength across all specimen types, establishing a straightforward yet robust predictive relationship for long-term strength estimation. Second, the 1:1 composite configuration demonstrated the greatest creep longevity, along with the smallest instantaneous and time-dependent strains and the lowest steady-state creep rate among all composite specimens—collectively identifying this ratio as an optimal configuration for creep resistance. Third, as the proportion of rock increased, the relative contribution of shear cracking declined while tensile cracking became progressively dominant, reflecting a transition in failure mechanism from shear-controlled to tension-controlled behavior. Correspondingly, both the crack initiation stress and the crack damage stress thresholds followed a non-monotonic trend, reaching peak values at K_{rc} = 1:1 before declining at higher rock fractions. Taken together, these results provide quantitative guidance for the rational design of coal pillar geometries and the assessment of long-term structural stability in underground mining operations.

Keywords: rock-to-coal height ratio; combinations; long-term strength; acoustic emission characteristics

List of symbols

K_{rc}	Rock-to-coal height ratio
σ_c	Peak strength
σ_{cr}	Creep failure stresses
σ_{ls}	Long-term strength
σ_{ci}	Crack initiation stress
σ_{cd}	Crack damage stress
ε_{is}	Instantaneous strain
ε_{cs}	Creep strain

V_{sc}	Steady-state creep rate
SEM	Scanning electron microscopy
AE	Acoustic emission
AF	Average frequency
RA	Rising angle

1. Introduction

Retaining protective coal pillars constitutes a critical engineering measure in both underground coal mining—where they provide roof support within goafs—and open-pit operations, where they serve to stabilize highwall slopes against deformation and structural failure (Wang et al., 2025; Zhang et al., 2017). Structurally, these pillars function as composite systems comprising coal seams and their immediately overlying roof strata. Subject to the sustained self-weight of the overburden, such coal–rock assemblages undergo prolonged stress loading, which drives time-dependent creep deformation and may ultimately precipitate catastrophic instability—manifesting as roof collapse or slope sliding, both of which rank among the most severe engineering geological hazards in mining practice. Of the numerous parameters governing the mechanical response of coal–rock composites, the K_{rc} is arguably the most consequential. A systematic characterization of how K_{rc} modulates creep behavior and crack evolution therefore requires dedicated experimental investigation across a range of ratio configurations, combining creep loading protocols with acoustic emission (AE) monitoring. The outcomes of such work carry dual significance: at the theoretical level, they advance the mechanistic understanding of time-dependent failure in heterogeneous rock–coal systems; at the applied level, they yield quantitative criteria to inform the rational dimensioning of coal pillars in deep underground stopes and open-pit end slopes, as well as to support the long-term stability assessment of existing pillar structures.

Coal–rock combinations represent fundamental load-bearing structures in mining engineering, the mechanical behavior and long-term stability of which bear directly on operational safety during coal extraction. Substantial progress has been achieved in characterizing the mechanical response of such composites through both laboratory experimentation and theoretical analysis. Among the variables examined, specimen configuration has received considerable attention, with prior investigations concentrating predominantly on macro- and meso-scale mechanical responses as functions of compositional arrangement, strength contrast, and height ratio. Representative investigations (F. Li et al., 2022; Z. Li et al., 2023; Yu et al., 2022) characterized the uniaxial mechanical properties, energy evolution, and failure modes of three structural configurations—rock–coal (R–C), rock–coal–rock (R–C–R), and coal–rock (C–R)—and established through comparative analysis that the R–C–R arrangement yields superior uniaxial mechanical performance relative to the remaining two. The governing role of the rock-to-coal strength contrast on composite deformation and strength was subsequently demonstrated(W. Guo et al., 2022; Zhao et al., 2021) : failure preferentially initiates within the weaker constituent, and the overall strength of the assembly converges toward that of the weaker component. Along a parallel line of inquiry, the influence of height ratio on macro-scale mechanical properties and meso-scale structural characteristics was examined (Ke et al., 2025; Wang et al., 2020) , revealing a direct dependence of composite strength on K_{rc}—specifically, an increase in rock thickness consistently elevates the overall

strength of the assembly. Beyond these configurational effects, the fundamental mechanical behaviors of coal–rock composite structures have been systematically characterized across a broad range of loading conditions (Cheng et al., 2020; Wang et al., 2024). The mechanical behavior of coal–rock composite structures has been shown to depend substantially on K_{rc} (Chen et al., 2020; Ma et al., 2021; Wang et al., 2020) . A higher rock proportion markedly enhances the pre-peak energy storage capacity of the assembly, with the accumulated strain energy becoming progressively concentrated within the coal constituent. At the interface scale, the contact properties between coal and rock exert a profound influence on compressive strength, shear strength, permeability, failure mode, and overall macroscopic mechanical response (Gu et al., 2022; Tian et al., 2022; Wang et al., 2023; Zhao et al., 2015). The role of structural inclination has also been addressed: as the dip angle increases, both the peak strength and long-term strength of coal decline in a nonlinear fashion, while the dominant creep failure mechanism transitions from tensile splitting toward combined tensile–shear damage (C. Li et al., 2022; Yufeng, 2020). For damage characterization of composite structures, acoustic emission (AE) monitoring has been widely adopted given its capacity to capture internal damage evolution in real time. An investigation into AE and infrared signals during the failure of composites with varying height ratios revealed a negative correlation between pre-failure AE counts and peak AE counts, alongside a positive correlation between cumulative AE counts and K_{rc} (Hao et al., 2024) . A separate study demonstrated how K_{rc} modulates AE energy release and governs the operative failure mechanisms through systematic analysis of AE responses across composites of differing height ratios (D. Guo et al., 2022) . Building on this foundation, the failure and energy evolution characteristics of composites were further elucidated under the combined effects of height ratio, moisture content, and constituent material type, through integrated mechanical testing and AE monitoring (Cai et al., 2025; Yao et al., 2020).

Despite the substantial body of knowledge accumulated on the constituent elements, mechanical characteristics, and damage monitoring of coal–rock composites, existing studies have largely been confined to mechanical responses and instantaneous failure mechanisms under conventional loading rates. A systematic investigation into the deformation laws, strength attenuation characteristics, and instability evolution of coal–rock composites under long-term sustained loading—i.e., creep conditions—remains conspicuously lacking. Furthermore, while K_{rc} has been firmly established as a core variable governing the static mechanical performance and energy distribution of the composite, the manner in which it regulates long-term creep behavior, together with the underlying mechanisms driving creep damage accumulation, remains an open question warranting dedicated inquiry. To bridge these knowledge gaps, this study conducts scanning electron microscopy (SEM), uniaxial stepwise creep tests on coal–rock composites with varying K_{rc} values, complemented by real-time AE monitoring throughout the loading process. The influence of K_{rc} on the time-dependent mechanical behavior of the composites

is systematically examined from three complementary perspectives: axial deformation characteristics, creep rate evolution, and long-term strength degradation. AE response characteristics are subsequently correlated with the observed creep behavior to elucidate the crack initiation, propagation, and coalescence mechanisms operative under different height ratio conditions. Ultimately, the findings of this work are intended to provide a rigorous theoretical foundation for the rational geometric design of coal pillars in underground stopes and open-pit end slopes, as well as for the comprehensive assessment of their long-term structural stability.

2. Experimental System and Test Scheme

2.1 Specimen Preparation

The composite specimens were categorized into five groups according to their respective K_{rc} values: pure coal (C, K_{rc} = 0:1), three composite configurations (R1C3, K_{rc} = 1:3; R1C1, K_{rc} = 1:1; R3C1, K_{rc} = 3:1), and pure sandstone (R, K_{rc} = 1:0). Coal and sandstone blocks were sequentially cored, cut, and ground into standard cylindrical specimens of varying heights to achieve the designated height ratios. All end faces were precision-polished to ensure that parallelism and flatness tolerances remained within 0.05 mm and 0.02 mm, respectively. For the composite groups, sandstone and coal cylinders were bonded in a "rock-on-coal" configuration using white latex adhesive. The resulting bonding interface was verified to possess a shear strength of approximately 2.5 MPa, a value that exceeds the tensile strengths of both coal (0.6 MPa) and sandstone (1.8 MPa), thereby ensuring that failure initiates within the constituent materials rather than at the interface itself. A minimum of three specimens was prepared for each group, and the complete experimental scheme is summarized in Table 1.

Table 1 Experimental Scheme

The test groups	rock height(mm)	K_{rc}	dimensions（mm × mm）
C	0	0 ： 1	φ50×100
R1C3	25	1 ： 3	φ50×100
R1C1	50	1 ： 1	φ50×100
R3C1	75	3 ： 1	φ50×100
R	100	1 ： 0	φ50×100

2.2 Experimental System and Method

A VEGA3 SEM was employed to examine the microstructural characteristics of both coal and rock specimens. Creep loading and damage monitoring were carried out using an integrated testing system comprising an MTS816 rock mechanical testing machine coupled with a Micro-II Express AE acquisition system. The corresponding experimental procedure is depicted in Figure 1. A stepwise loading protocol was adopted, with the stress levels at each stage determined on the basis of prior uniaxial compressive strength (UCS) test results. The mechanical parameters and corresponding stress loading levels derived

from the unconfined compression tests are summarized in Table 2. The specific testing procedure was as follows: force-controlled loading was applied at a constant ramp rate of 0.02 MPa/s with a data acquisition frequency of 10 Hz. Each specimen was loaded progressively until the prescribed stepwise stress level was attained, whereupon the load was held constant to allow sufficient creep deformation to develop. Upon stabilization of the creep response, the subsequent stage of axial compression loading was initiated. This stepwise procedure was repeated until the specimen ultimately underwent creep failure.

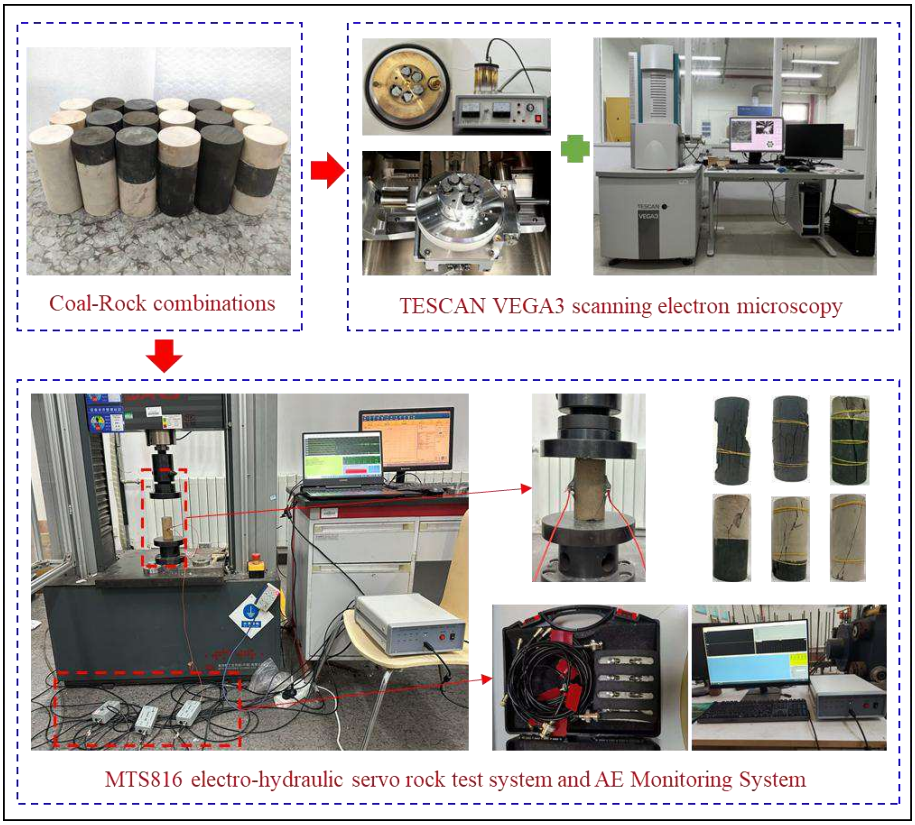


Figure 1 Experimental System

Table 2 Mechanical Parameters of Unconfined Compression Tests and Creep Test Scheme

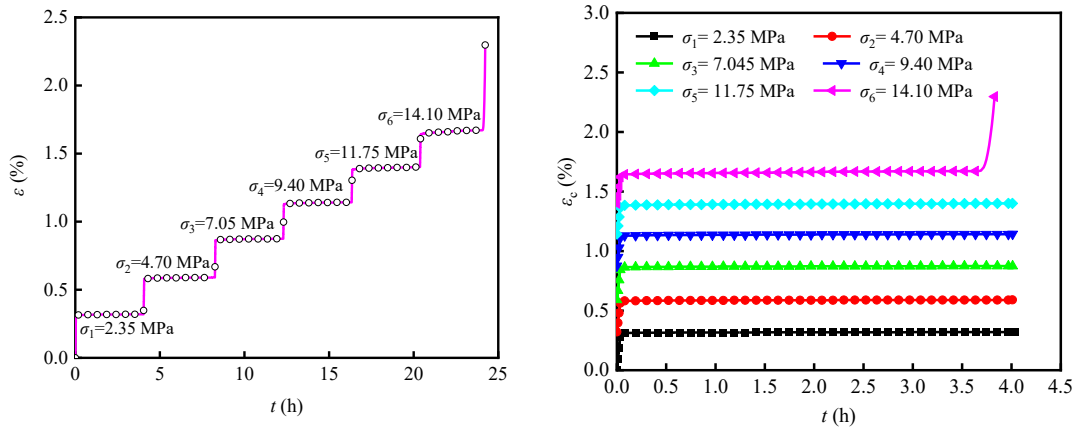
Test Group	Peak Strength (σ_c) / Mpa	Peak Strain /%	First-Stage Stress Level / Mpa	Incremental Stress Increase / Mpa	Creep Loading Duration / h
C	15.65	1.53	2.35	$0.15\sigma_c$	4
R1C3	17.58	1.42	2.64	$0.15\sigma_c$	4
R1C1	20.43	1.39	3.06	$0.15\sigma_c$	4
R3C1	22.81	1.33	3.42	$0.15\sigma_c$	4
R	31.05	1.2	4.66	$0.15\sigma_c$	4

3. Results

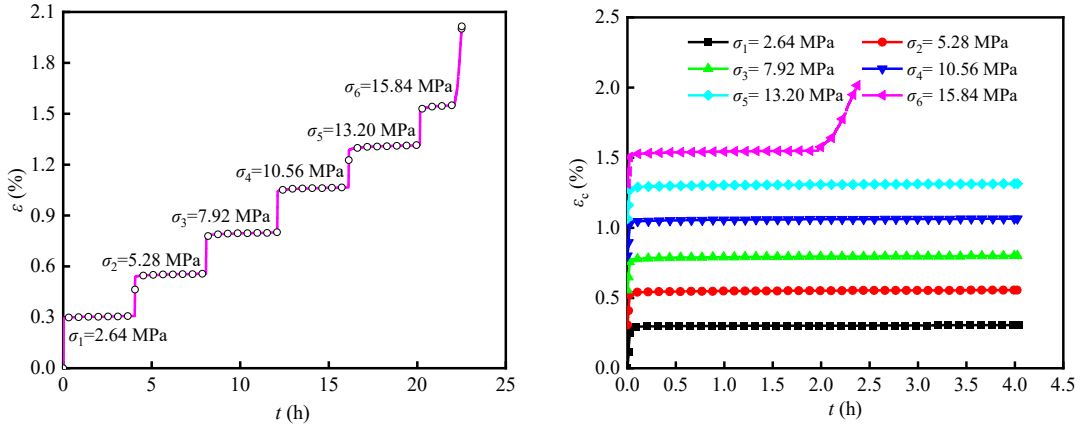
3.1 Axial Deformation Characteristics

The axial creep time-history curves of the composite specimens are presented in Figure 2. It can be observed that all specimens exhibited three characteristic creep stages: decelerating creep, steady-state creep, and accelerating creep. The axial strain increased in a stepwise manner over time, with pronounced

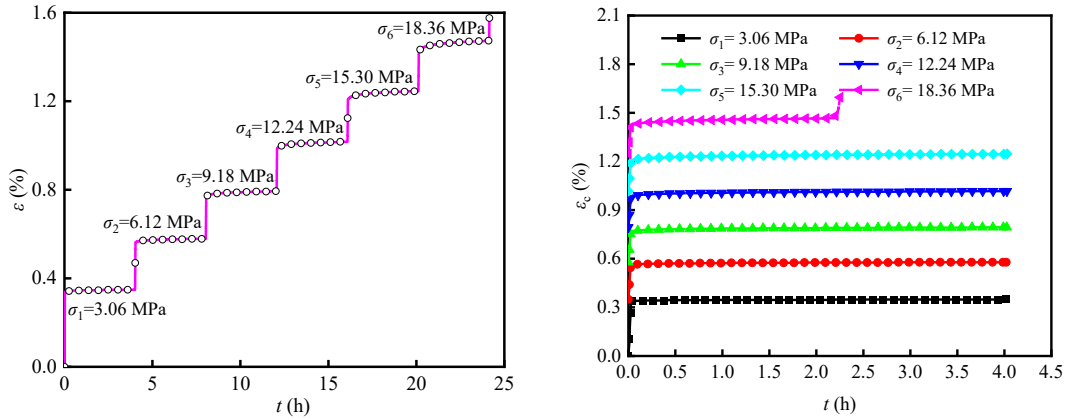
instantaneous deformation occurring at the onset of each loading stage. Under the final applied stress level, all composite specimens transitioned sequentially from the steady-state creep stage into the accelerating creep stage, ultimately culminating in creep failure, and displayed broadly consistent deformation patterns in their overall creep curves. For K_{rc} values of 0:1, 1:3, 1:1, 3:1, and 1:0, the creep failure stresses (σ_{cr}) of specimens C, R1C3, R1C1, R3C1, and R were 14.10, 15.84, 18.36, 20.52, and 27.96 MPa, respectively, with corresponding creep failure times of 24.23, 22.51, 24.14, 23.15, and 21.72 h. Notably, as the proportion of rock in the composite increased, σ_{cr} exhibited a monotonically increasing trend, and the ratio of σ_{cr} to the uniaxial compressive strength σ_c remained approximately 90% across all groups. Among the composite specimens, the creep failure times of R1C3, R1C1, and R3C1 ranged from 21.72 to 24.23 h. Of all the composite groups, specimen R1C1 (K_{rc} = 1:1) recorded the longest creep failure time, suggesting that a balanced rock-to-coal height ratio induces the most prolonged time-dependent damage accumulation prior to ultimate failure.



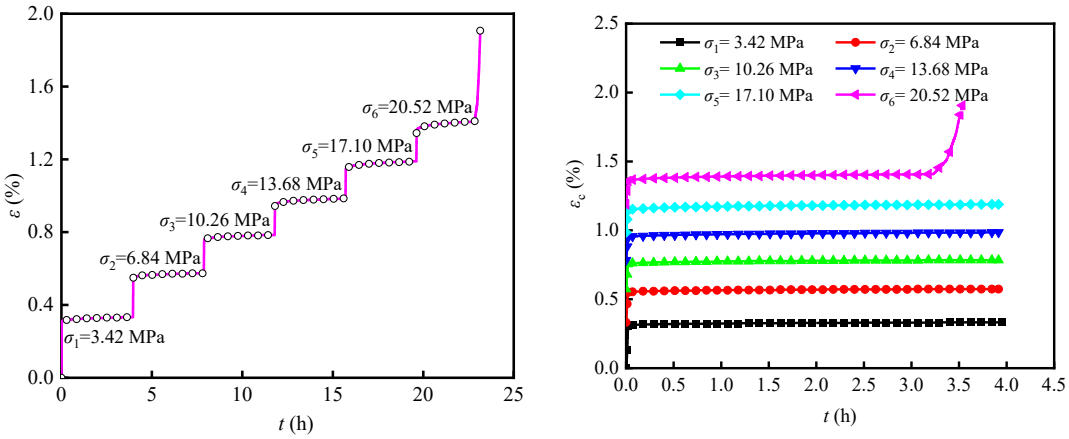
（a）C



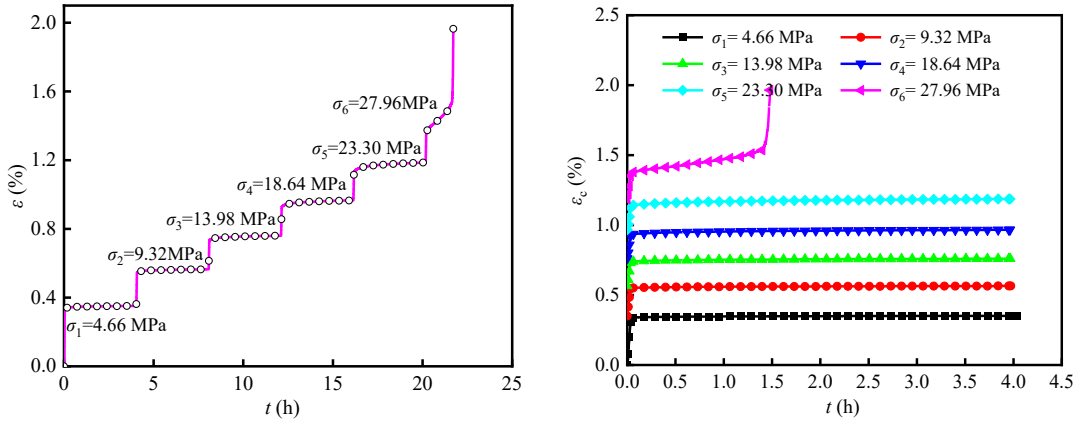
（b）R1C3



（c）R1C1



（d）R3C1



（e）R

Figure 2 Creep time-history curves of specimens

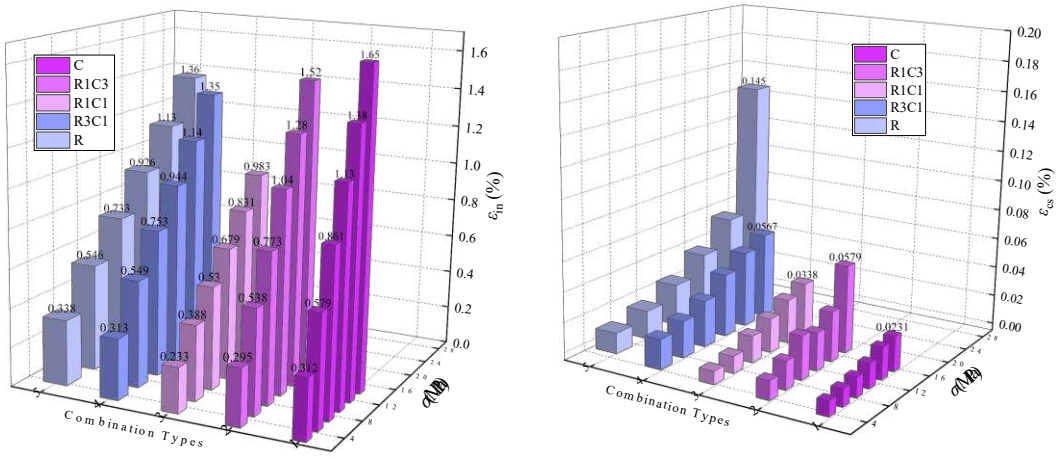
To more thoroughly characterize the creep deformation behavior of the composite specimens, the creep curves were subjected to further decomposition, whereby the total strain accumulated during creep was partitioned into two components: instantaneous strain (ε_{is}) and creep strain (ε_{cs}) Specifically, ε_{is} denotes the strain generated instantaneously upon the application of each incremental stress level, whereas ε_{cs} represents the additional strain increment accumulated while the applied stress was held constant. The relationships between ε_{is}, ε_{cs}, and the corresponding stress levels for the pure coal,

composite, and pure sandstone specimens are illustrated in Figure 3.

As revealed by Figure 3(a), in the longitudinal direction (Y-direction), the ε_{is} of all composite specimens increased approximately linearly with rising stress levels. In the lateral direction (X-direction), the ε_{is} of composite specimens displayed a characteristic "high–low–high" trend, whereby as the proportion of rock progressively increased, ε_{is} first decreased and subsequently rebounded. Among all specimens, R1C1 consistently recorded the minimum ε_{is} at each corresponding stress level.

As shown in Figure 3(b), in the Y-direction, the ε_{cs} of composite specimens exhibited a general upward trend with increasing stress levels. At the final stress level, the ε_{cs} values of specimens C, R1C3, R1C1, R3C1, and R were 0.0231%, 0.0579%, 0.0338%, 0.0567%, and 0.145%, respectively. Notably, the pure coal specimen recorded the smallest ε_{cs}, while the pure sandstone specimen recorded the largest. Among the composite groups ε_{cs} followed a non-monotonic pattern, first decreasing and then increasing with increasing rock proportion, with R1C1 exhibiting the minimum value. In the X-direction, the ε_{cs} of composite specimens R1C3, R1C1, and R3C1 similarly displayed a "high–low–high" distribution: as the rock proportion increased, ε_{cs} first decreased and then increased, again with R1C1 attaining the minimum among all composite groups. Taken together, when K_{rc} = 1:1, specimen R1C1 exhibited the smallest ε_{is} and ε_{cs} among all composite groups, a finding that is physically consistent with the observation that R1C1 also recorded the longest creep failure time reported earlier.

In summary, the incorporation of sandstone into the composite system effectively enhanced the overall mechanical performance of the composite specimens. Relative to pure coal specimens, the composites exhibited notably higher uniaxial compressive strength σ_c and σ_{cr}, accompanied by a reduction in ε_{is}. Relative to pure sandstone specimens, the composites demonstrated a prolonged creep failure time and a reduced ε_{cs}. It is noteworthy that, while the introduction of sandstone consistently improved the mechanical performance of the composites, the specific creep properties were further governed by the K_{rc}. Experimental results revealed that at K_{rc} = 1:1, composite specimen R1C1 achieved the most favorable combination of creep-related properties, representing the optimal overall performance among all composite configurations investigated.

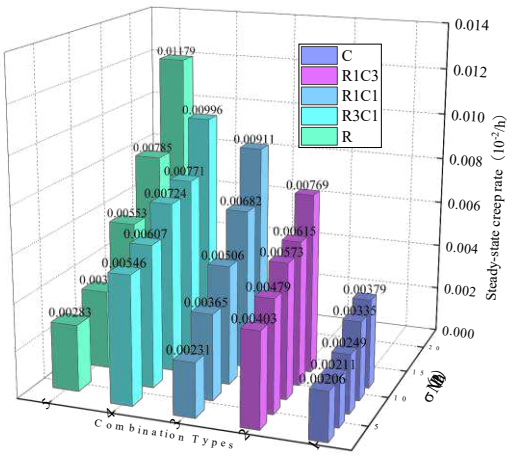


(a) composite specimens ε_{is} (b) composite specimens ε_{cs}

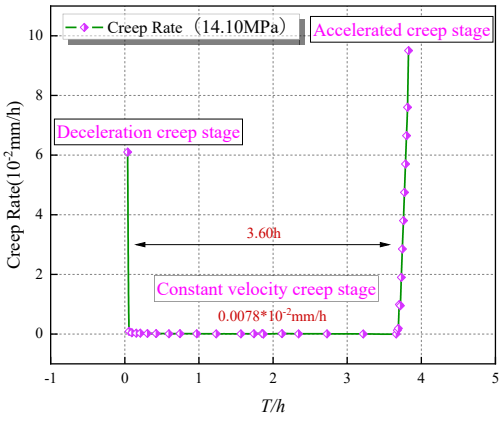
Fig. 3 ε_{is} and ε_{cs} of specimens

3.2 Creep Rate Characteristics

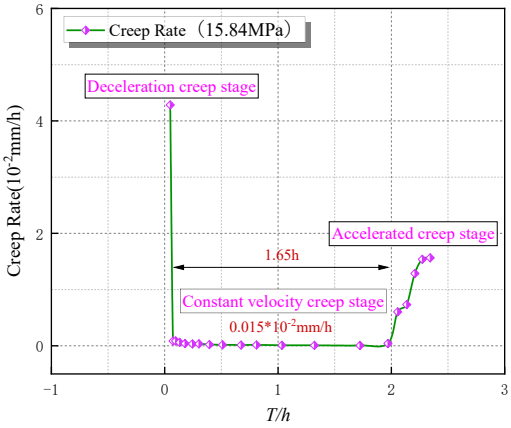
Figure 4(a) presents the steady-state creep rate (V_{sc}) at each stress level prior to the ultimate failure stress σ_{cr}. As observed from Figure 4(a), prior to reaching σ_{cr}, the variation pattern of V_{sc} with stress level was essentially consistent across all composite specimens, with V_{sc} increasing monotonically as the stress level rose. As illustrated in Figures 4(b) to (f), which depict the creep rate evolution curves of composite specimens under the final applied stress σ_{cr}, the specimen deformation rate exhibited three distinct temporal stages: decelerating creep, constant-rate (steady-state) creep, and accelerating creep. Accordingly, the creep rate of the specimen demonstrated a characteristic evolutionary pattern of initial rapid decrease, subsequent stabilization, and final rapid acceleration. The V_{sc} values of specimens C, R1C3, R1C1, R3C1, and R were 0.00780×10^{-2}, 0.0150×10^{-2}, 0.0123×10^{-2}, 0.0125×10^{-2}, and 0.0981×10^{-2} mm/h, respectively, with the corresponding durations of the constant-rate creep stage being 3.60 h, 1.65 h, 1.93 h, 3.16 h, and 1.36 h. Notably, under the final stress level, V_{sc} exhibited a "high–low–high" distribution pattern across the composite specimens, with R1C1 recording the minimum steady-state creep rate. This distribution pattern was generally consistent with the previously observed variation trend of ε_{cs} at the final stress level. The duration of the constant-rate creep stage for all composite specimens ranged from 1.36 h to 3.60 h. Specifically, at the ultimate stress level, the duration of the constant-rate creep stage for the composite groups was intermediate between that of the pure rock specimen (shortest) and the pure coal specimen (longest). Furthermore, as the proportion of rock in the composite increased, the duration of the constant-rate creep stage demonstrated a progressively increasing trend.



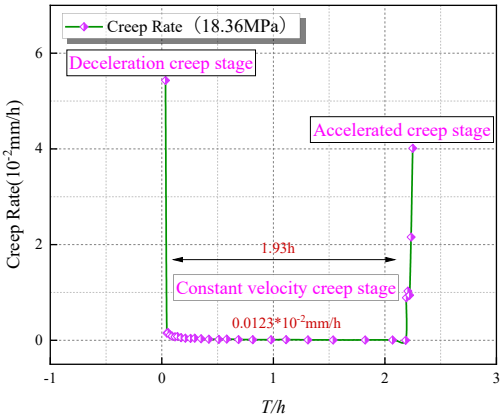
（a）Steady-state Creep Rate



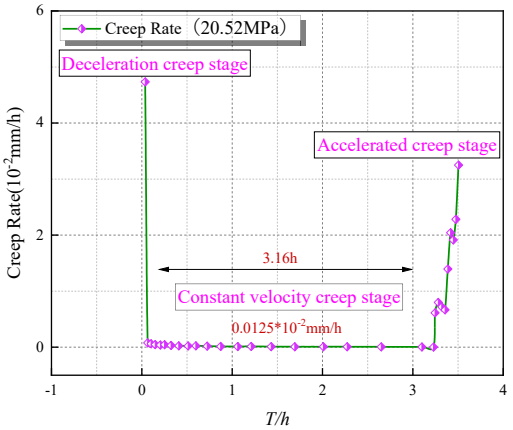
（b）C



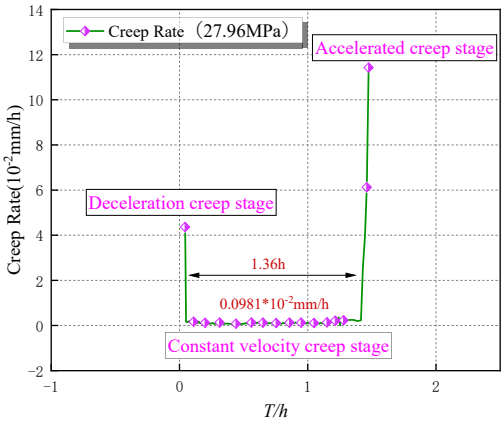
（c）R1C3



（d）R1C1



（e）R3C1



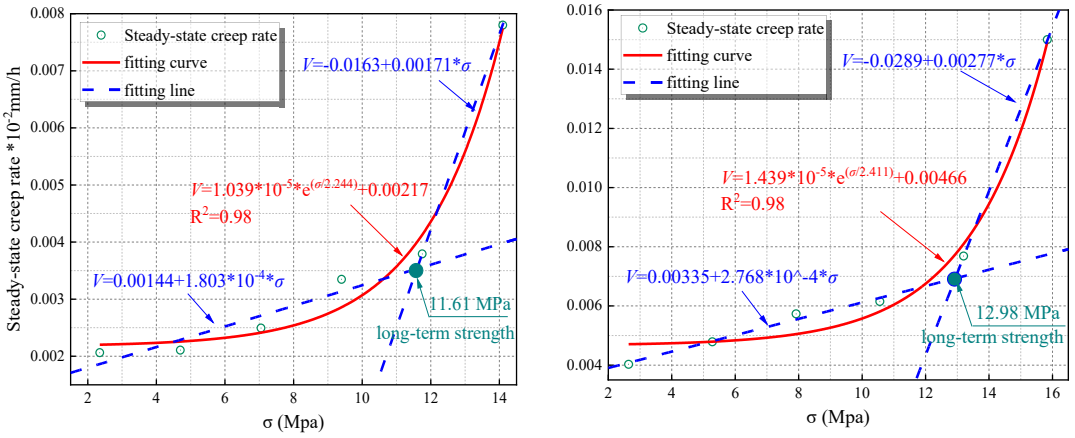
（f）R

Figure 4 Creep rates of specimens

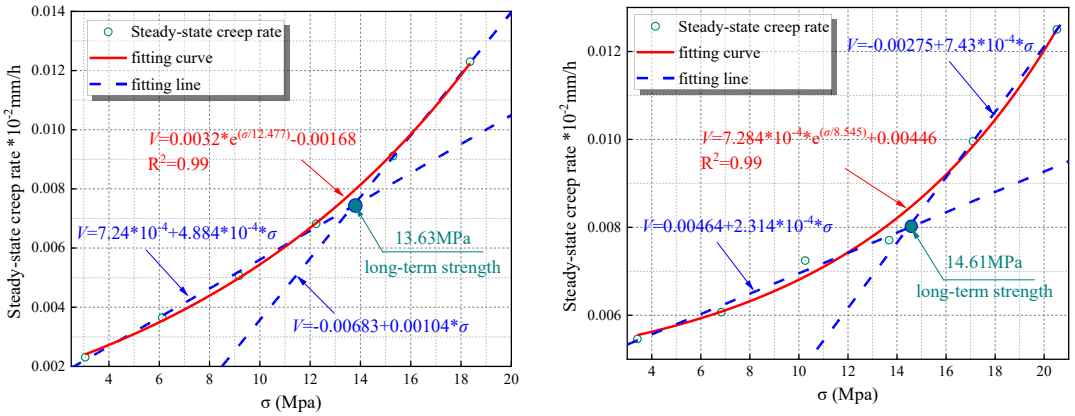
3.3 Long-term Strength Characteristics

The steady-state creep rate method was employed in this investigation to determine the long-term strength of the composite specimens. Specifically, the creep rate-stress relationship data for each composite specimen were plotted, and linear regression fitting was subsequently applied to the data

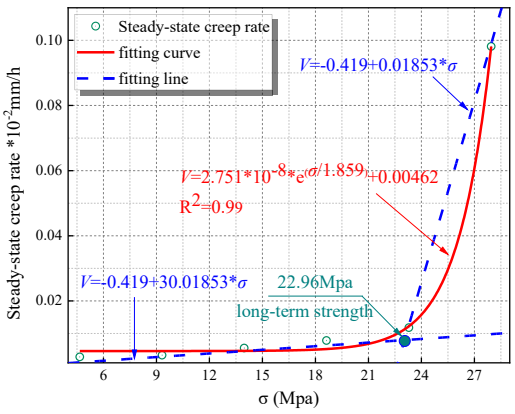
segments on either side of the inflection point in the creep rate-stress curve. The abscissa coordinate of the intersection point between the two fitted linear functions corresponded to the long-term strength (σ_{ls}) of the specimen(X. Li et al., 2023).



（a）C　　（b）R1C3



（c）R1C1　　（d）R3C1



（e）R

Figure 5 Long-term strength characteristics of composite specimens

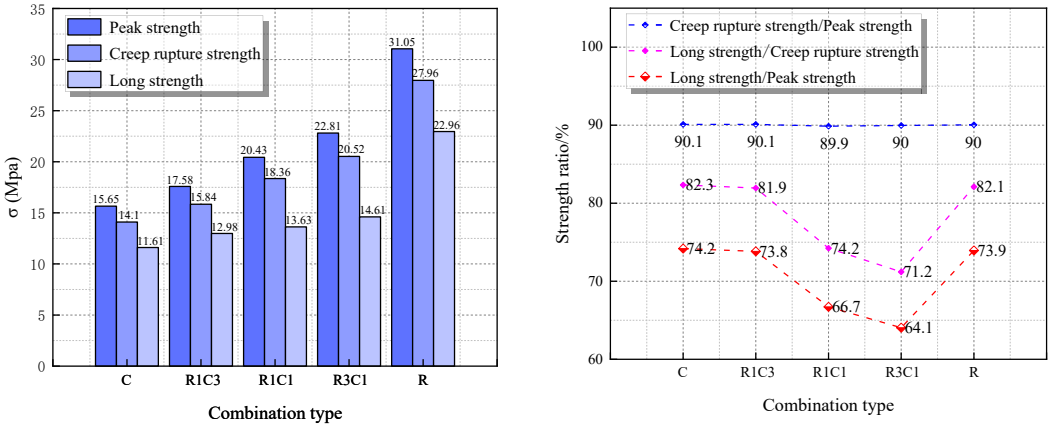
As illustrated in Figures 5(a)–(e), exponential functions were utilized to fit the steady-state creep rate V_{sc} data of the composite specimens, and all coefficient of determination (R^2) values exceeded 0.98.

This excellent fit quality indicated that, across varying K_{rc} configurations, the steady-state creep rate V_{sc} of composite specimens increased exponentially with progressively increasing stress levels. The long-term strength (σ_{ls}) values of specimens C, R1C3, R1C1, R3C1, and R were 11.6, 12.98, 13.63, 14.61, and 22.96 MPa, respectively.

Figure 6(a) presents the variation of uniaxial compressive strength σ_c, creep failure stress σ_{cr}, and long-term strength σ_{ls} as a function of rock proportion in the composite specimens. It was observed that as the rock proportion increased, all three strength parameters—σ_c , σ_{cr}, and σ_{ls}—showed consistent improvement, with the specimen strengths following the hierarchical order $\sigma_c > \sigma_{cr} > \sigma_{ls}$.

As shown in Figure 6(b), under varying K_{rc}, the variation trends of the ratios σ_{ls}/σ_c and σ_{ls}/σ_{cr} for composite specimens exhibited identical patterns, both displaying a characteristic "decline-then-rise" behavior. Specifically, the ratios of σ_{ls} to σ_c were 74.2%, 73.8%, 66.7%, 64.1%, and 73.9%, respectively; the corresponding ratios of σ_{ls} to σ_{cr} were 82.3%, 81.9%, 74.2%, 71.2%, and 82.1%, respectively; and the ratios of σ_{cr} to σ_c were 90.1%, 90.1%, 89.9%, 90%, and 90%, respectively.

In conclusion, across varying K_{rc} configurations, the ratio of σ_{cr} to σ_c for composite specimens remained approximately constant at 90%, demonstrating that this fundamental strength relationship was independent of rock proportion. Consequently, the creep failure stress σ_{cr} and long-term strength σ_{ls} of composite specimens can be reliably predicted based on their measured uniaxial compressive strength σ_c.



(a)σ_{ls} , σ_{cr} , σ_c (b) Strength ratios

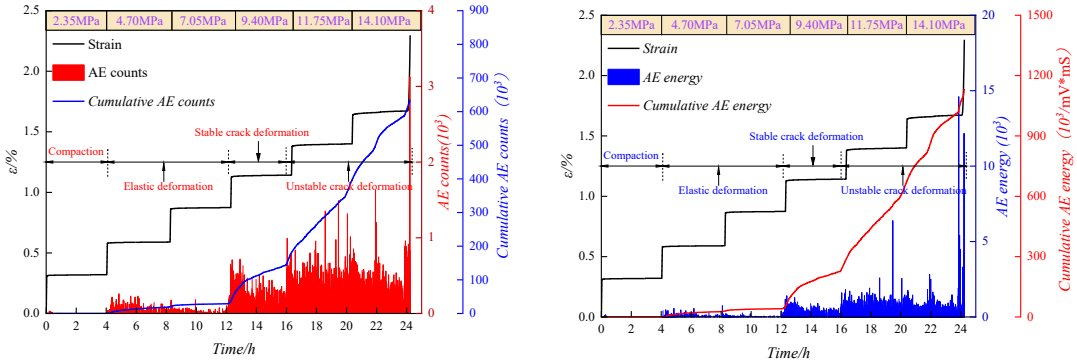
Figure 6 Strength and strength ratios of specimens

3.4 AE Characteristics During Creep Failure

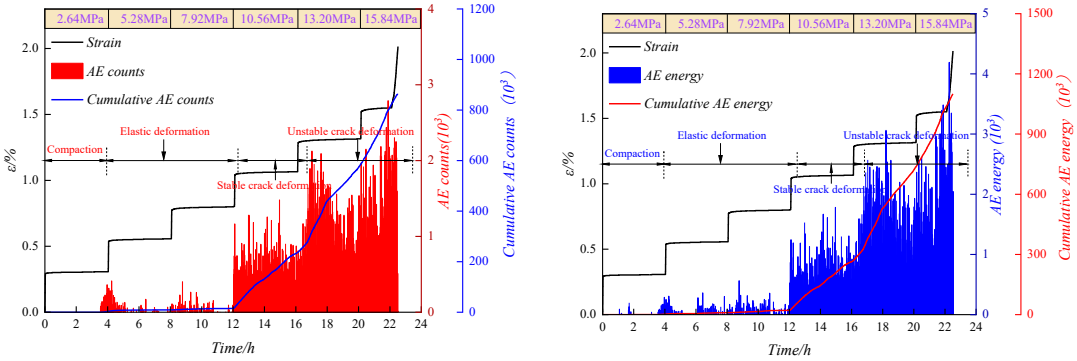
AE ring count and energy are fundamental parameters that characterize the frequency and intensity of AE events, thereby providing direct insight into the evolution process of internal microcracks within the specimen.(Yang et al., 2024). As illustrated in Figure 7, the crack evolution of the specimen during

uniaxial creep can be delineated into four distinct phases: crack compaction, elastic deformation, stable crack propagation, and unstable crack propagation. The AE ring count and cumulative energy of composite specimens generally exhibited a progressively increasing trend as the applied stress level increased, independent of the specific K_{rc} configuration. Taking specimen C as an illustrative example, at a relatively low applied stress of 2.35 MPa, both the AE ring count and cumulative energy remained low, indicating that the number of micro-fractures generated within the specimen was minimal and the energy released was correspondingly limited. At this stress level, which fell below the critical stress threshold required for fracture initiation, no apparent macroscopic fracture damage was observed in the specimen. However, owing to the inherent heterogeneity of coal as a material, a few sporadic AE events still occurred. During this phase, the cumulative AE ring count and energy curves displayed modest slopes, and this stage could be appropriately designated as the AE calm period, corresponding to the crack compaction stage of the specimen's mechanical response. As the applied stress increased to the range of 2.35–7.05 MPa, although the growth amplitude remained modest, both the AE ring count and cumulative energy showed incremental increases relative to the preceding stage. As newly formed cracks gradually developed and propagated, the slopes of the cumulative curves correspondingly increased. This intermediate stage could be designated as the AE low-amplitude growth period, corresponding to the elastic deformation stage of the specimen. At higher applied stresses of 9.40–14.10 MPa, the AE ring count and cumulative energy exhibited pronounced surges, accompanied by a dramatic steepening of the curve slopes. During this phase, numerous microcracks formed, coalesced, and propagated at accelerated rates. This stage, which encompasses both the stable and unstable crack propagation phases of the specimen's mechanical response, could be appropriately designated as the AE high-amplitude growth period.

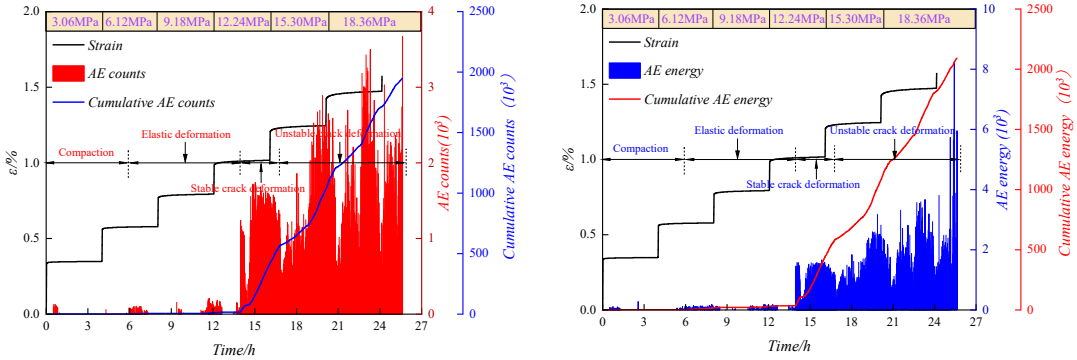
In summary, the AE ring count and cumulative energy data from specimen C provided direct quantitative reflection of its progressive damage evolution process. Consequently, the employment of AE monitoring signals to forecast the creep deformation behavior and damage accumulation of coal-rock composite specimens under sustained loading is critically imperative for ensuring the long-term mechanical stability and safety of underground mine pillars and supporting structures.



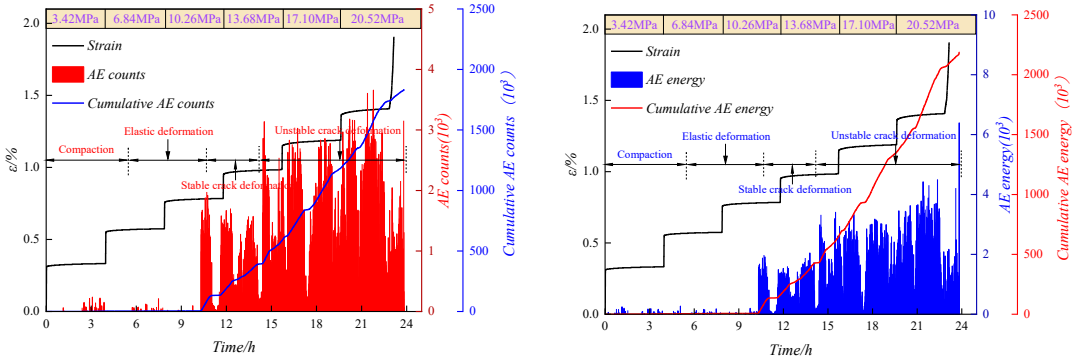
（a）C



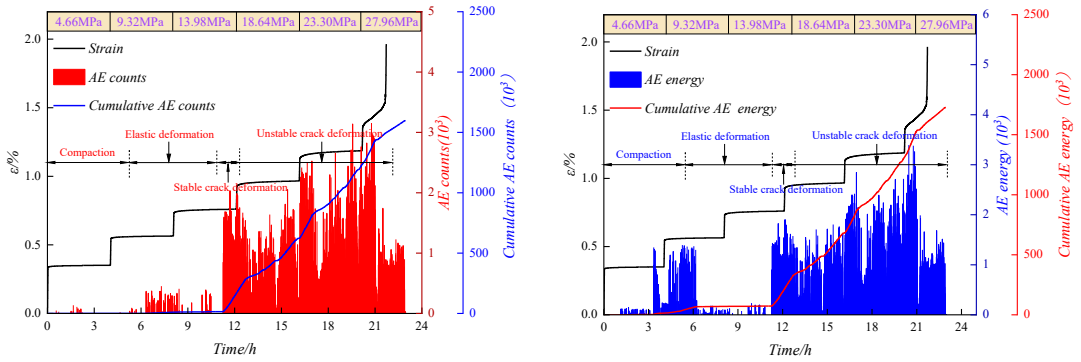
（b）R1C3



（c）R1C1



（d）R3C1



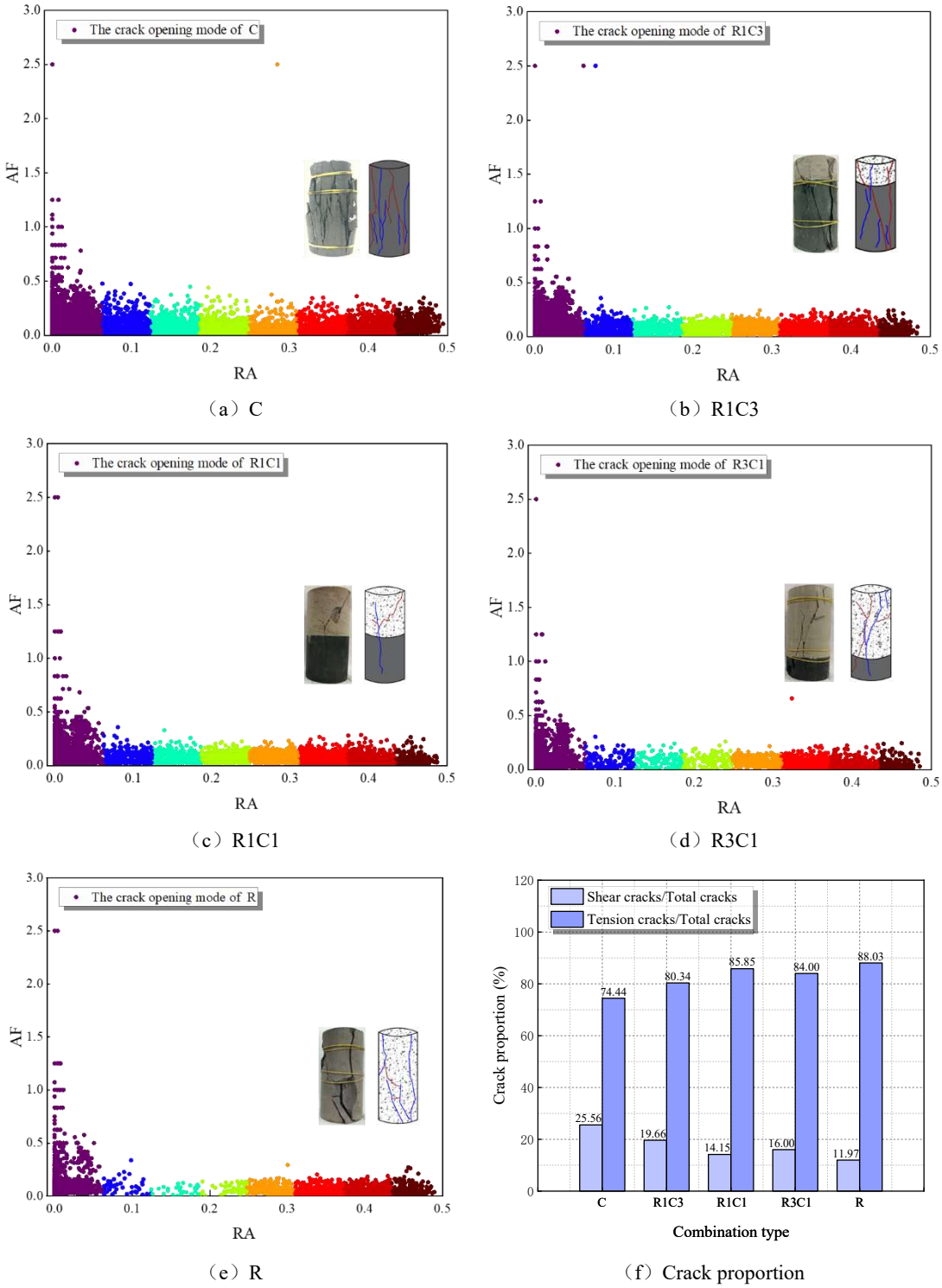
（e）R

Figure 7 Ring count and energy characteristics of composite specimens

To gain deeper insight into the formation and development of interior microcracks in composite specimens, the average frequency (*AF*) and rising angle (*RA*) were employed as characterization parameters for quantifying the evolution of internal microcrack patterns in composite specimens. The *RA* and *AF* values for the specimens were calculated from fundamental AE parameters, specifically rise time and signal amplitude. As illustrated in Figure 8, the *RA* and *AF* values exhibited a dense clustering pattern near the coordinate axes, with the maximum *RA* value not exceeding 0.5. As the rock proportion increased progressively, the composite specimens demonstrated a consistent reduction in the overall percentage contribution of shear cracks, accompanied by a complementary increase in the percentage of tensile cracks. Notably, in specimens R1C3, R1C1, and R3C1, the percentage of shear cracks exhibited a characteristic "initial decline followed by rebound" pattern.

Specifically, when the specimen consisted of pure coal (Specimen C), multiple prominent main cracks spanning across the upper and lower end faces were visibly observed on the specimen surface following failure. The percentage distribution of crack types were: tensile cracks accounting for 74.44% and shear cracks for 25.56%. As the K_{rc} increased to 1:3, the damage severity of composite R1C3 decreased noticeably, with a reduction in surface macroscopic cracks. The corresponding percentages of tensile and shear cracks were 80.34% and 19.66%, respectively. As the K_{rc} further increased to 1:1, the damage level of R1C1 continued to decrease, accompanied by a significant reduction in surface macroscopic cracks. The percentages of tensile and shear cracks were 85.85% and 14.15%, respectively, indicating the most favorable crack distribution pattern. As the K_{rc} increased to 3:1, the damage degree of composite R3C1 intensified compared to R1C1, with a notable increase in the number of surface macroscopic cracks. The percentages of tensile and shear cracks were 84% and 16%, respectively. When the specimen consisted of pure rock (Specimen R), the damage pattern was substantially more severe,

with macroscopic cracks penetrating across the entire specimen volume. Tensile and shear cracks accounted for 88.03% and 11.97%, respectively, indicating pronounced crack propagation throughout the specimen.



（a）C （b）R1C3

（c）R1C1 （d）R3C1

（e）R （f）Crack proportion

Figure 8 AF-RA relationship, macroscopic fracture, and tensile-shear crack proportion variation of specimens

4. Discussion

4.1 Influence Mechanism of K_{rc} on Strength of Composite Specimens

The observed increase in both creep failure strength (σ_{cr}) and long-term strength (σ_{ls}) with increasing rock proportion (Figure 6a) can be explained by two interacting mechanisms.

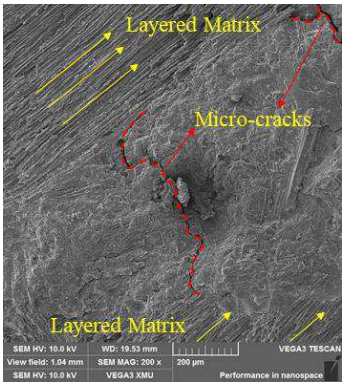
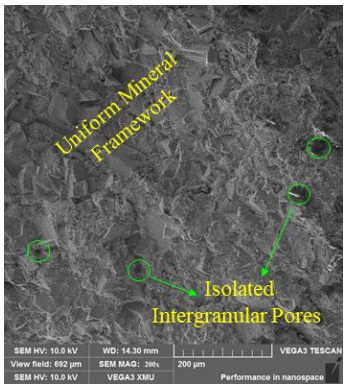
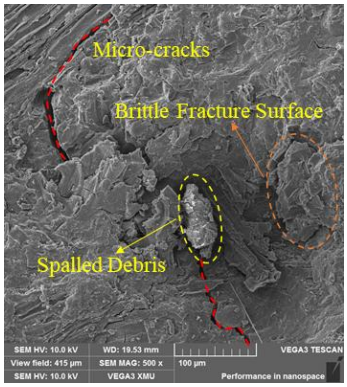
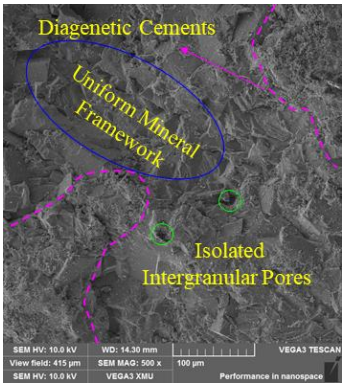
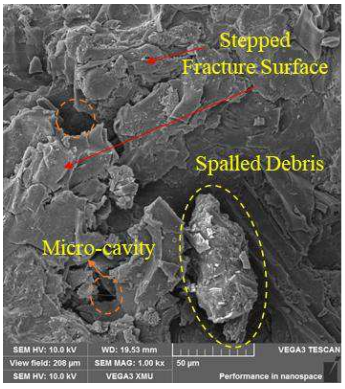
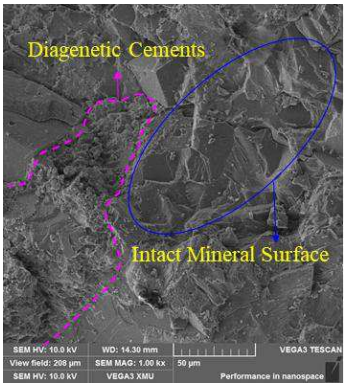
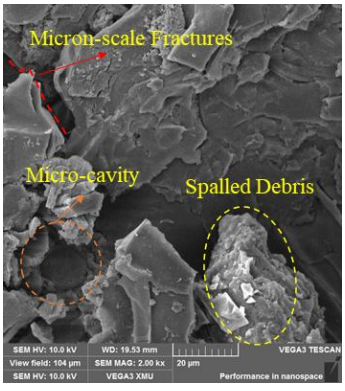
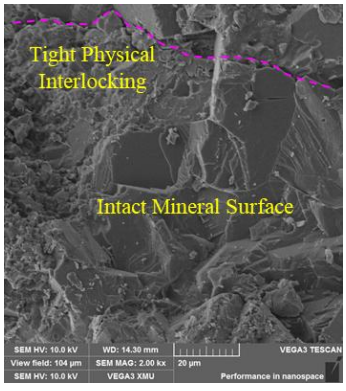
First, the coal component inherently contains abundant natural defects, whereas the sandstone component exhibits substantially greater structural integrity. To directly verify this fundamental hypothesis, systematic SEM observations were performed on fresh fracture surfaces of unloaded coal and sandstone specimens at magnifications ranging from 200× to 2000× (Table 3). The coal microstructure exhibits evident fragmentation and irregularly distributed spalling pits. Pore and microcrack widths range from several micrometers to tens of micrometers. Many of these pores are interconnected by pre-existing, densely distributed microcracks, forming a complex microdefect network that greatly facilitates stress concentration and substantially accelerates creep damage accumulation. In contrast, the sandstone microstructure consists of a rigid mineral grain skeleton with tightly interlocked crystalline texture, presenting a macroscopically dense and uniform appearance. Although some well-developed intergranular pores are visible, almost no through-going microcracks are observed. These microstructural differences directly support the first mechanistic explanation: with increasing sandstone proportion, the volume fraction of defect-rich (fractured and fragmented) material in the composite is effectively reduced. Owing to its exceptional structural integrity and rigid support, the sandstone component significantly enhances the strength and long-term mechanical stability of the composite.

Second, the stiffer rock layer laterally constrains the coal layer through shear stress transferred across the interface. This confinement suppresses the lateral expansion of coal under axial compression, reducing the deviatoric stress within the coal and delaying the onset of unstable crack growth. Importantly, this confinement effect is optimal when the rock and coal layers have comparable thickness (K_{rc} = 1:1). At this ratio, the interfacial shear stress is sufficiently high to constrain coal deformation but not high enough to cause premature interface debonding. This explains why the R1C1 composite exhibits the longest creep life and the smallest instantaneous and creep strains among all composites.

Furthermore, the ratio of long-term strength to peak strength (σ_{ls}/σ_c) first decreases and then increases with increasing rock proportion (Figure 6b), with the minimum occurring at K_{rc} = 1:1. This non-monotonic behavior suggests that at the optimal height ratio, the composite benefits most from synergistic interlayer interaction. However, the relative reduction in long-term strength (compared to peak strength) is actually more pronounced. In other words, the 1:1 composite achieves higher absolute strengths, but its strength degrades more significantly under sustained loading. This subtle trade-off

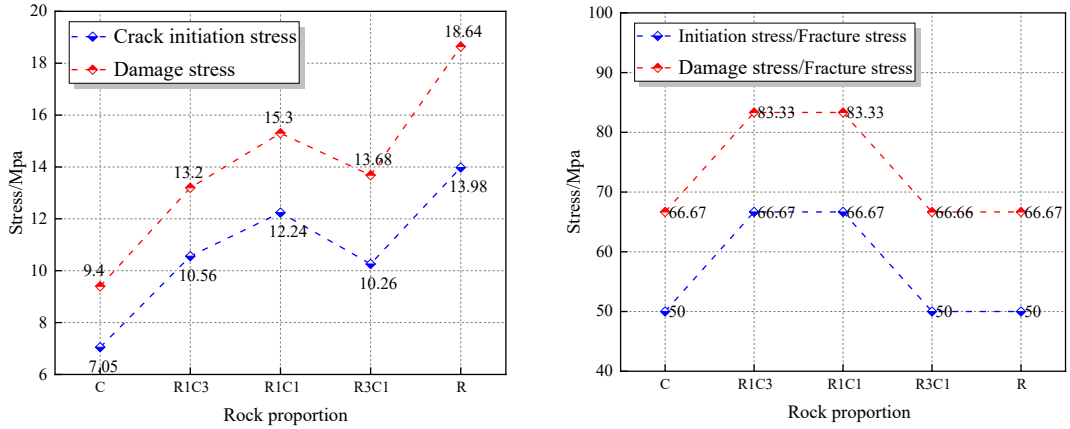
should be considered in engineering design.

Table 3 SEM images of coal and sandstone specimens at different magnifications

Image magnification	Coal sample	Sandstone sample
200x		
500x		
1000x		
2000x		

4.2 Evolution Law of Microcracks in Composite Specimens Under Different K_{rc}

Based on the AE ring count and energy characteristics (Figure 7), the microcrack evolution process can be divided into four stages: crack compaction, elastic deformation, stable crack propagation, and unstable crack propagation. The crack initiation stress (σ_{ci}) and crack damage stress (σ_{cd}) were identified from the inflection points in the cumulative AE ring count curve. Figure 9a shows that σ_{ci} and σ_{cd} for the five specimen groups (C, R1C3, R1C1, R3C1, R) are 7.05, 10.56, 12.24, 10.26, 13.98 MPa and 9.40, 13.20, 15.30, 13.68, 18.64 MPa, respectively. Both thresholds exhibit a non-monotonic dependence on K_{rc}: they first increase from C to R1C1, then decrease from R1C1 to R3C1, and finally increase again for pure rock. The 1:1 composite (R1C1) shows the highest σ_{ci} and σ_{cd} among the composite groups.



(a) σ_{ci} and σ_{cd} of composite specimens

(b) Ratios of σ_{ci}, σ_{cd} to creep failure stress of composite specimens

Figure 9 Stress and stress ratio variation of specimens

Figure 9b presents the ratios of σ_{ci} and σ_{cd} to the creep failure stress σ_{cr}. The σ_{ci} /σ_{cr} ratios are 0.50, 0.67, 0.67, 0.50, and 0.50 for C, R1C3, R1C1, R3C1, and R, respectively. The σ_{cd} /σ_{cr} ratios are 0.67, 0.83, 0.83, 0.67, and 0.67. Notably, the R1C3 and R1C1 composites exhibit higher threshold ratios (0.67 and 0.83) than the pure coal, pure rock, and the 3:1 composite, all of which have ratios of 0.50 and 0.67. This indicates that introducing a thin rock layer (1:3) or an equal-thickness rock layer (1:1) can effectively elevate the stress levels at which microcracks initiate and coalesce, thereby expanding the elastic and stable crack growth regimes. However, when the rock layer becomes too thick (3:1), the benefit diminishes, likely because the thick rock layer imposes excessive constraint that induces stress concentration at the interface or within the coal near the interface.

The RA-AF analysis (Figure 8) provides further insight into the crack type transition. With increasing rock proportion, the proportion of shear cracks progressively decreases (25.56% for C, 19.66% for R1C3, 14.15% for R1C1, 16% for R3C1, 11.97% for R), while the proportion of tensile cracks

increases accordingly. This shift from shear-dominated to tension-dominated failure is consistent with the macroscopic failure modes shown in Figure 8: pure coal exhibits multiple steep shear fractures, while pure rock displays vertical splitting (tensile) cracks. For composites, the failure mechanism is intermediate. At the 1:1 ratio, the specimen shows the fewest macroscopic cracks and the lowest shear crack proportion among composites, indicating that the balanced constraint promotes a more uniform tensile-dominated damage pattern that is less likely to trigger rapid instability. This explains why the R1C1 specimen has the longest creep life: a tensile-dominated crack network propagates more stably than a shear-dominated one, delaying the onset of accelerating creep.

In summary, K_{rc} regulates both the strength thresholds and the crack evolution mode. The 1:1 ratio optimizes the balance between constraint and deformation compatibility, resulting in the highest crack initiation and damage stresses, the widest stable crack growth stage, and a predominantly tensile failure mechanism, all of which contribute to superior creep resistance.

5. Conclusions

Based on a comprehensive series of systematic uniaxial stepwise creep tests, SEM observations, and real-time AE monitoring conducted on coal-rock composite specimens with varying rock-to-coal height ratios (K_{rc} = 0:1, 1:3, 1:1, 3:1, 1:0), the following principal conclusions are drawn:

(1) Constant ratio of creep failure strength to peak strength: For all specimens, regardless of K_{rc}, the creep failure stress is approximately 90% of the peak strength. This simple relationship enables reliable prediction of long-term strength from short-term uniaxial compression tests.

(2) Optimal height ratio for creep resistance and mechanical stability: Among the composite specimens, the 1:1 ratio (R1C1) exhibits the longest creep life, the smallest instantaneous and creep strains, and the lowest steady-state creep rate. This optimal performance results from a balanced interfacial constraint that maximizes suppression of coal lateral expansion without inducing premature interface debonding.

(3) Transition of failure mechanism with increasing rock proportion: As the rock proportion increases, the proportion of shear cracks progressively decreases while that of tensile cracks increases. The crack initiation stress and the crack damage stress both first increase and then decrease, peaking at K_{rc} = 1:1. These observations indicate a shift from shear-dominated to tension-dominated failure, with the 1:1 ratio providing the widest stable crack growth stage.

Declarations

Funding

This work was financially supported by the National Natural Science Foundation of China (52474159、52304102), the Xinjiang Uygur Autonomous Region Science and Technology Major Program (No. 2023A01002), the Ordos major science and technology program (select the best candidates to undertake key research projects) (JBGS-2023-003), the Xuzhou Key Research and Development Plan (Social Development), Project Number: KC23314.

References:

Cai, Y., Zhou, X., Wang, L., Fu, Q., & Li, Q. (2025). Mechanical Damage Characteristics and Energy Evolution Laws of Primary Coal – Rock Combinations with Different Coal – Rock Ratios *Applied Sciences* (15, pp.).

Chen, G., Qin, Z., Zhang, G., Li, T., & Li, J. (2020). Law of energy distribution before failure of a loaded coal-rock combined body. *Rock and Soil Mechanics*, 41(06), 2021-2033. http://doi.org/10.16285/j.rsm.2019.0101

Cheng, Z., Li, L., & Zhang, Y. (2020). Laboratory investigation of the mechanical properties of coal-rock combined body. *Bulletin of Engineering Geology and the Environment*, 79(4), 1947-1958. http://doi.org/10.1007/s10064-019-01613-z

Gu, X., Guo, W., Zhang, C., Zhang, X., Guo, C., & Wang, C. (2022). Effect of interfacial angle on the mechanical behaviour and acoustic emission characteristics of coal – rock composite specimens. *Journal of Materials Research and Technology*, 21, 1933-1943. http://doi.org/https://doi.org/10.1016/j.jmrt.2022.09.104

Guo, D., Zhang, W., Chen, Q., & Wang, Z. (2022). Failure Mechanism and Acoustic Emission Characteristics of Coal – Rock Samples. *Journal of Mining Science*, 58(3), 390-397. http://doi.org/10.1134/S106273912203005X

Guo, W., Zhang, D., Zhao, T., Li, Y., Zhao, Y., Wang, C., & Wu, W. (2022). Influence of Rock Strength on the Mechanical Characteristics and Energy Evolution Law of Gypsum – Rock Combination Specimen under Cyclic Loading – Unloading Condition. *International Journal of Geomechanics*, 22(5), 4022034. http://doi.org/10.1061/(ASCE)GM.1943-5622.0002276

Hao, T., Wang, G., Li, F., Tang, Y., & Yuan, M. (2024). Study on the characteristics of acoustic-thermal precursors of destabilization damage in coal-rock combination bodies with different proportions. *Scientific Reports*, 14(1), 25661. http://doi.org/10.1038/s41598-024-77170-7

Ke, F., Chen, Y., Wu, P., Zhou, Y., Zhang, P., Dong, J., & Jiao, Y. (2025). Influence of coal-rock height ratio on the mechanical properties and crack evolution patterns of combined coal-rock bodies. *Journal of Cleaner Production*, 490, 144793. http://doi.org/https://doi.org/10.1016/j.jclepro.2025.144793

Li, C., He, S., Xu, Z., & Yan, F. (2022). Experimental Investigation on Long-Term Strength and Acoustic Emission Characteristics of Coal Pillar under Inclined Compression Loading. *Geofluids*, 2022, 1213215. http://doi.org/10.1155/2022/1213215

Li, F., Yin, D., Wang, F., Jiang, N., & Li, X. (2022). Effects of combination mode on mechanical properties of bi-material samples consisting of rock and coal. *Journal of Materials Research and Technology*, 19, 2156-2170. http://doi.org/https://doi.org/10.1016/j.jmrt.2022.05.174

Li, X., Liu, X., Tan, Y., Chen, A., Wang, H., Wang, X., & Yang, S. (2023). Rheological mechanical properties and its constitutive relation of soft rock considering influence of clay mineral composition and content. *International Journal of Coal Science & Technology*, 10(1), 48. http://doi.org/10.1007/s40789-023-00615-3

Li, Z., Zhang, G., Li, Y., Zhou, W., Qin, T., Zeng, L., & Liu, G. (2023). Energy Accumulation Law of Different Forms of Coal – Rock Combinations *Energy Accumulation Law of Different Forms of Coal – Rock Combinations* (13, pp.).

Ma, Q., Tan, Y., Liu, X., Zhao, Z., & Fan, D. (2021). Mechanical and energy characteristics of coal – rock composite sample with different height ratios: a numerical study based on particle flow code.

Environmental Earth Sciences, 80(8), 309. http://doi.org/10.1007/s12665-021-09453-5

Tian, C., Sun, H., Dai, L., Li, R., Wang, B., Cao, J., Wang, J., Hu, Q., & Xin, L. (2022). Experimental Study on Mechanical Properties and Energy Evolution Law of Coal-Rock Composite Structure under Different Interface Connection Modes. *Geofluids*, 2022, 1288463. http://doi.org/10.1155/2022/1288463

Wang, K., Wang, L., Du, F., Zhao, W., Dong, H., Guo, Y., & Ju, Y. (2023). Evolutionary mechanism of permeability of coal-rock combination considering interface effect: Model development and analysis. *Energy*, 284, 129305. http://doi.org/https://doi.org/10.1016/j.energy.2023.129305

Wang, T., Ma, Z., Gong, P., Li, N., Cheng, S., & Yin, Z. (2020). Analysis of Failure Characteristics and Strength Criterion of Coal-Rock Combined Body with Different Height Ratios. *Advances in Civil Engineering*, 2020, 8842206. http://doi.org/10.1155/2020/8842206

Wang, W., Wang, K., Zhang, X., Jiang, Y., Cai, T., Yan, J., & Yue, S. (2024). Mechanical properties of coal-rock combined bodies under the action of ScCO2: A study of damage and failure mechanism. *Engineering Failure Analysis*, 156, 107807. http://doi.org/https://doi.org/10.1016/j.engfailanal.2023.107807

Wang, X., Xia, Z., Yao, Q., Li, X., Xu, Q., & Zhu, L. (2025). Numerical investigation of coal pillar damage mechanisms for various width-to-height ratios. *Scientific Reports*, 15(1), 2705. http://doi.org/10.1038/s41598-025-85554-6

Yang, G., Chen, Y., Xie, Q., Wu, P., & Zhang, Y. (2024). Physical and mechanical characteristics deterioration and crack evolution of sandy mudstone in an open-pit mine under multiple freeze–thaw cycles. *Geomechanics and Geophysics for Geo-Energy and Geo-Resources*, 10(1), 87. http://doi.org/10.1007/s40948-024-00808-3

Yao, Q., Wang, W., Zhu, L., Xia, Z., Tang, C., & Wang, X. (2020). Effects of moisture conditions on mechanical properties and AE and IR characteristics in coal–rock combinations. *Arabian Journal of Geosciences*, 13(14), 615. http://doi.org/10.1007/s12517-020-05610-5

Yu, W., Bao, P., Ke, L., & Shen, W. (2022). Mechanical properties and fracture evolution law of rock-coal-rock combination. *Journal of China Coal Society*, 47(03), 1155-1167. http://doi.org/10.13225/j.cnki.jccs.xr21.1563

Yufeng, F. (2020). Mechanical properties of coal rock combinations and evaluation of impact tendency considering effects of the height portion of coal. *Journal of China Coal Society*, 45(S2), 649-659. http://doi.org/10.13225/j.cnki.jccs.2019.1213

Zhang, J., Huang, P., Zhang, Q., Li, M., & Chen, Z. (2017). Stability and control of room mining coal pillars—taking room mining coal pillars of solid backfill recovery as an example. *Journal of Central South University*, 24(5), 1121-1132. http://doi.org/10.1007/s11771-017-3515-8

Zhao, T., Gu, X., Guo, W., Gong, X., Xiao, Y., Kong, B., & Zhang, C. (2021). Influence of rock strength on the mechanical behavior and P-velocity evolution of coal-rock combination specimen. *Journal of Materials Research and Technology*, 12, 1113-1124. http://doi.org/https://doi.org/10.1016/j.jmrt.2021.03.059

Zhao, Z., Wang, W., Wang, L., & Dai, C. (2015). Compression–shear strength criterion of coal–rock combination model considering interface effect. *Tunnelling and Underground Space Technology*, 47, 193-199. http://doi.org/https://doi.org/10.1016/j.tust.2015.01.007

校对报告

当前使用的样式是 [APA 7th]

当前文档题录总数为25条，在13个位置共计插入26次（包括重复插入）

有0条题录存在必填字段内容缺失的问题

所有题录的数据正常